Letter

High-precision measurements and first-principles explanation of the temperature-dependent ^{13}C and ^{14}N hyperfine interactions of single NV$^-$ centers in diamond at room temperature

Shaoyi Xu,[1,2,*] Mingzhe Liu,[1,2,*] Tianyu Xie,[1,2,†] Zhiyuan Zhao,[1,2] Qian Shi,[1,2] Pei Yu,[1,2] Chang-Kui Duan,[1,2,3,‡] Fazhan Shi,[1,2,3,4] and Jiangfeng Du[1,2,3,§]

[1]*CAS Key Laboratory of Microscale Magnetic Resonance and School of Physical Sciences, University of Science and Technology of China, Hefei 230026, China*

[2]*CAS Center for Excellence in Quantum Information and Quantum Physics, University of Science and Technology of China, Hefei 230026, China*

[3]*Hefei National Laboratory, University of Science and Technology of China, Hefei 230088, China*

[4]*School of Biomedical Engineering and Suzhou Institute for Advanced Research, University of Science and Technology of China, Suzhou 215123, China*

(Received 14 September 2022; accepted 21 March 2023; published 5 April 2023)

Revealing the properties of single spin defects in solids is essential for quantum applications based on solid-state systems. However, it is intractable to investigate the temperature-dependent properties of single defects, due to the low precision for single-defect measurements in contrast to defect ensembles. Here we report that the temperature dependence of the Hamiltonian parameters for single negatively charged nitrogen-vacancy centers in diamond at room temperature is precisely measured and the results are in reasonable agreement with first-principles calculations. In particular, the hyperfine interactions with randomly distributed ^{13}C nuclear spins are clearly observed to vary with temperature and the relevant coefficients are measured with hertz-level precision. The temperature-dependent behaviors are attributed to both thermal expansion and lattice vibrations by first-principles calculations. Our results pave the way for taking nuclear spins as more stable thermometers at nanoscale. The methods developed here for high-precision measurements and first-principles calculations can be further extended to other solid-state spin defects.

DOI: 10.1103/PhysRevB.107.L140101

I. INTRODUCTION

Accurate knowledge of the properties of spin defects in solids [1] is the basis for finding their applications in quantum sensing [2] and quantum computation and networks [3]. Measuring the susceptibilities of the target defect to external perturbations such as magnetic field, electric fields, strains, and temperature enables the detection of these quantities and the analysis of the decoherence resulting from their fluctuations. As one of the most prominent systems, the nitrogen-vacancy (NV) center in diamond, with its various properties carefully investigated [4], has acquired several remarkable achievements, including single-molecule magnetic resonance [5–7], nanoscale magnetic [8–10] and temperature [11,12] imaging, and multinode quantum networks [13,14].

With regard to the temperature dependence of the NV properties, in early works, the zero-field splitting (ZFS) is found to be temperature dependent [15–18], which enables the NV center to work as a nanoscale thermometer [11,12,19]. Recently, the temperature dependence of the hyperfine interactions with the surrounding ^{14}N and ^{13}C nuclear spins was also explored based on NV ensembles [20–23], which can provide more information on the temperature dependence of the spin-density distribution of the single negatively charged nitrogen-vacancy (NV$^-$) ground state. However, it is almost impossible to observe the temperature-dependent behaviors of the ^{13}C hyperfine interactions for these NV-ensemble-based works, since the ^{13}C atoms are randomly distributed in the proximity of the NV center.

In this work we utilize single NV centers to investigate the temperature dependence of the parameters involved in the ground-state Hamiltonian of the NV$^-$ center at room temperature. By performing Ramsey interferometry, the temperature dependence of the nearby ^{13}C spins with the coupling strengths 13.7, 12.8, −8.9, and −6.5 MHz is clearly observed and the temperature coefficients are measured with hertz-level precision. Furthermore, first-principles calculations are performed based on density-functional theory (DFT) [24–29] and the calculation results explain the experimental values fairly well. The temperature dependence of the hyperfine interactions is identified as the effects of both thermal expansion and lattice vibrations. Our methods combining high-precision measurements and first-principles calculations are generally applicable for other defects in solids such as phosphorus dopants in silicon [30], silicon vacancies in silicon carbide [31], cerium ions in yttrium aluminium garnet [32], and ytterbium ions in yttrium orthovanadate [33].

*These authors contributed equally to this work.
†xie1021@ustc.edu.cn
‡ckduan@ustc.edu.cn
§djf@ustc.edu.cn

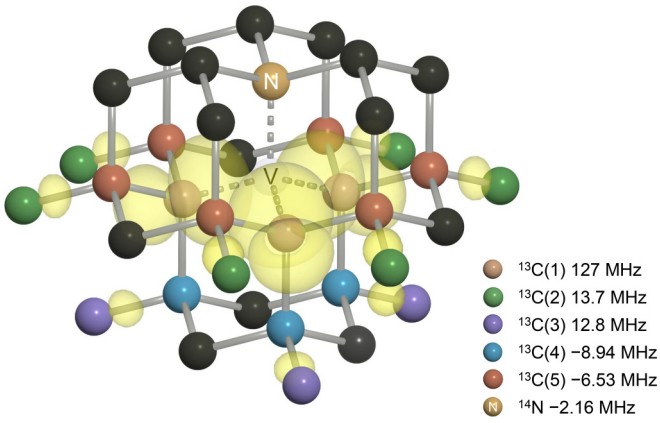

FIG. 1. Atomic structure of the NV center in a diamond lattice and the calculated spin-density distribution. The dark yellow sphere denotes the nitrogen atom, while the white one represents the vacancy. The other spheres except the dark ones denote the carbon atoms studied in this work with the coupling strengths displayed in the legend. The spin density of the NV center spreads across multiple lattice sites and interacts with the nearby ^{14}N and ^{13}C nuclear spins through magnetic dipolar moments. The distribution of the spin density is calculated based on DFT.

II. SYSTEM AND METHODS

The NV center in diamond lattice consists of a substitutional ^{14}N atom and an adjacent vacancy, as shown in Fig. 1(a). The electronic state studied here is the ground state of the NV$^-$ spin triplet [4]. Two temperature-dependent phenomena in solids, i.e., thermal expansion and lattice vibrations, both have significant perturbations on the distribution of the ground-state waveform that determines the coupling parameters involved in the Hamiltonian concerning the NV electron spin and the nuclear spins. Thus, the nuclear spins, especially the ^{13}C spins on multiple lattice sites (Fig. 1(a)), can serve as atomic-scale sensors to probe the electron waveform and its variation with external perturbations, e.g., the temperature in this work. By constructing an optically detected magnetic resonance (ODMR) setup with temperature control [34] (see the Supplemental Material [35]), the temperature dependence of the coupling parameters for single NV$^-$ centers can be investigated.

The bulk diamonds used here are all ultrapure with ^{13}C natural abundance (see the Supplemental Material [35]). Considering the hyperfine interactions with the ^{14}N nuclear spin [46] and various ^{13}C nuclear spins [47,48], the ground-state Hamiltonian under a bias field $\mathbf{B}$ with taking the NV axis as the z direction can be formulated as

$$H_g = H_e + H_{\mathrm{N}} + H_{\mathrm{C}}, \tag{1}$$

$$H_e = D(T)S_z^2 + \gamma_e \mathbf{B}\cdot\mathbf{S}, \tag{2}$$

$$H_{\mathrm{N}} = P(T)\left(I_z^{\mathrm{N}}\right)^2 - \gamma_n^{\mathrm{N}}\mathbf{B}\cdot\mathbf{I}^{\mathrm{N}} + \mathbf{S}\cdot\mathbf{A}^{\mathrm{N}}(T)\cdot\mathbf{I}^{\mathrm{N}}, \tag{3}$$

$$H_{\mathrm{C}} = -\gamma_n^{\mathrm{C}}\sum_i \mathbf{B}\cdot\mathbf{I}_i^{\mathrm{C}} + \mathbf{S}\cdot\sum_i \mathbf{A}_i^{\mathrm{C}}(T)\cdot\mathbf{I}_i^{\mathrm{C}}, \tag{4}$$

where the temperature-dependent parameters include the ZFS of the NV spin $D(T)$, the quadrupole coupling $P(T)$ of the ^{14}N spin, the hyperfine interaction $\mathbf{A}^{\mathrm{N}}(T)$ of the ^{14}N spin, and $\mathbf{A}_i^{\mathrm{C}}(T)$ of the ^{13}C(i) spin; $\mathbf{S}$, $\mathbf{I}^{\mathrm{N}}$, and $\mathbf{I}_i^{\mathrm{C}}$ are the operators of the NV spin, the ^{14}N spin, and the ^{13}C(i) spin, respectively; and γ_e, γ_n^{N}, and γ_n^{C} are the gyromagnetic ratios of three kinds of spins. The coupling tensor $\mathbf{A}^{\mathrm{N}}(T)$ only has two independent parameters due to the C_{3v} symmetry, while the $\mathbf{A}_i^{\mathrm{C}}(T)$ has six.

In this work the temperature-dependent parameters described above can all be precisely determined by measuring the transition frequencies of the electron spin and the nuclear spins. First, the ZFS of the electron spin $D(T)$ in Eq. (2) can be easily obtained with kilohertz-level precision by performing pulsed ODMR spectra. Second, by using the method in [46], the quadrupole coupling $P(T)$ and the hyperfine interaction $\mathbf{A}^{\mathrm{N}}(T)$ in Eq. (3) can both be solved by measuring six nuclear transition frequencies with hertz-level precision under a field of approximately 510 G. As for the ^{13}C hyperfine interactions, although the tensor $\mathbf{A}_i^{\mathrm{C}}(T)$ in Eq. (4) cannot be fully solved due to its complexity, the temperature dependence can still be obtained by averaging two nuclear transition frequencies under a small bias field of 10–30 G with

$$A = \tfrac{1}{2}(\omega_{+1} + \omega_{-1}) = \sqrt{A_{zx}^2 + A_{zy}^2 + A_{zz}^2} + R, \tag{5}$$

where ω_{+1} and ω_{-1} are the transition frequencies of the ^{13}C spin in both $m_S = +1$ and -1 subspaces of the NV spin. The remainder term R (see the Supplemental Material [35]) is constant with the temperature if the bias field is stable enough, and thus measuring the mean A under different temperatures gives the temperature coefficient of the coupling term $\sqrt{A_{zx}^2 + A_{zy}^2 + A_{zz}^2}$.

III. EXPERIMENTS

In the following, the temperature dependence of the relevant parameters is measured experimentally based on the discussion above. At first, by performing pulsed ODMR spectra under different temperatures, the variation of the ZFS with the temperature is obtained as $-71.9(0.3)$ kHz/K for single NV centers at room temperature (see the Supplemental Material [35]). The deviation from the ensemble NV result $-74.2(0.7)$ kHz/K [15] may originate from the vast strain difference between the diamond samples used in two works or the systematic error for temperature measurements. Then, by applying the method [46] for measuring the quadrupole coupling $P(T)$ and the hyperfine interaction $\mathbf{A}^{\mathrm{N}}(T)$ of the ^{14}N nuclear spin, the temperature coefficients are given by 35.0(0.3) and 194.9(1.0) Hz/K (see the Supplemental Material [35]), in good agreement with the previous ensemble NV results [21–23].

The main challenge in the experiments is to measure the temperature dependence of the hyperfine interactions $\mathbf{A}^{\mathrm{C}}(T)$ for the ^{13}C nuclear spins in the proximity of single NV centers. Before the measurement, a small bias field of 10–30 G is applied and aligned to the NV axis by adopting the method of three-level quantum beat [49]. Figure 2 shows the measurement process by taking a ^{13}C(2) spin [Fig. 1(a)] as an example. Based on the level structure of the NV-^{13}C(2) coupled system shown in Fig. 2(a), the Ramsey sequence together with that

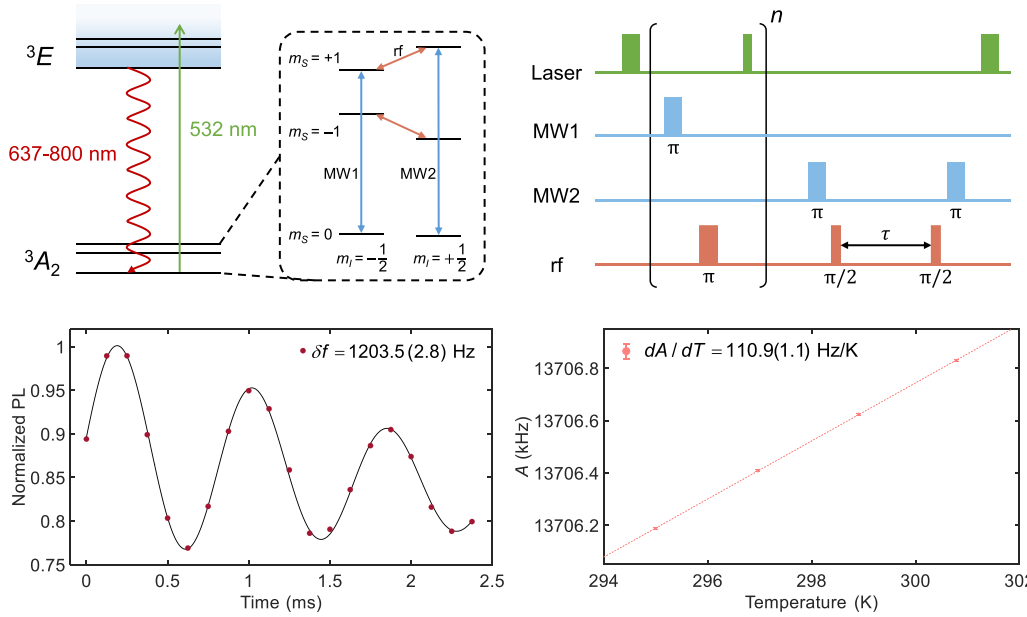

FIG. 2. Measurement for the temperature dependence of the hyperfine interaction of a ^{13}C(2) nuclear spin. (a) Level diagram for the NV center strongly coupled to a ^{13}C(2) nuclear spin. The 532-nm laser pulse is used to initialize the NV electron spin into the state $|m_S = 0\rangle$ and read out the spin state by collecting fluorescence photons with the (637–800)-nm phonon sideband. The orange arrows indicate the two nuclear transitions with the frequencies ω_{+1} and ω_{-1} in Eq. (5) to be measured, which are driven by radio-frequency (rf) pulses. The transitions for the NV electron spin, as indicated by the blue arrows, are driven by microwave (MW) pulses. The rf, MW1, and MW2 pulses are used in the pulse sequence in (b). (b) Pulse sequence of the laser, MW, and rf for Ramsey interference between the state $|m_S = +1, m_I = +\frac{1}{2}\rangle$ and the state $|m_S = +1, m_I = -\frac{1}{2}\rangle$. The sequence enclosed by the brackets is repeated n times to polarize the ^{13}C(2) spin into the state $|m_I = +\frac{1}{2}\rangle$. (c) Resultant interference pattern after applying the sequence in (b). The black line is plotted by fitting the data with the function $\{a \sin[2\pi(\delta f)t + \phi_0] + b\} \exp[-(t/T_2^*)^p] + c$, giving the detuning $\delta f = 1203.5(2.8)$ Hz. (d) Mean A of the two nuclear transition frequencies ω_{+1} and ω_{-1} measured under different temperatures. The temperature coefficient of the ^{13}C(2) nuclear spin at room temperature is given by 110.9(1.1) Hz/K with a linear fit.

for polarizing the ^{13}C(2) spin, as displayed in Fig. 2(b), is applied for measuring the ^{13}C(2) transition frequency ω_{+1} in the $m_S = +1$ subspace of the NV spin. The resulting interference pattern is plotted in Fig. 2(c) with the fitting curve. The value of 13 684 603.5(2.8) Hz for ω_{+1} is obtained by adding the detuning δf to the radio frequency used in the Ramsey sequence. By repeating the process above to acquire the transition frequencies ω_{+1} and ω_{-1} under different temperatures, the temperature coefficient for the ^{13}C(2) spin is given by 110.9(1.1) Hz/K, as shown in Fig. 2(d).

There are some other effects induced by varying the temperature inside the box, e.g., the drift of the bias field, and these effects may disturb the measurement results above. Therefore, in order to ensure that the measured temperature-dependent behaviors are indeed originated from the temperature dependence of the ^{13}C hyperfine interactions, the same experiments in Fig. 2 are implemented under three bias fields for two NV centers that are coupled to ^{13}C(3) nuclear spins. The results shown in Fig. 3 are identical within the error bars, which verifies the validity and robustness of the measurement method adopted in this work. The final temperature coefficients for four kinds of ^{13}C spins and the ^{14}N spin are given by averaging the results of 15 NV centers in four diamond samples (see the Supplemental Material [35]) and summarized in Fig. 4(d).

IV. FIRST-PRINCIPLES CALCULATIONS

Here we perform first-principles calculations to find reasonable explanations for the experimental results above. The coupling tensor $\mathbf{A}$ for a nuclear spin can be calculated at a given geometric structure by averaging the magnetic dipolar interaction [50] over the spin-density distribution of the NV^- ground state, which includes the isotropic Fermi contact term and the anisotropic dipolar term. In our first-principles

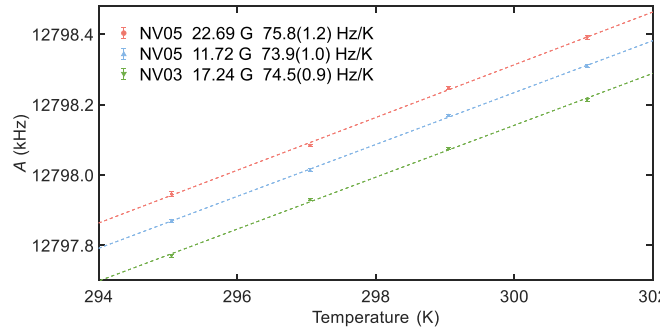

FIG. 3. Experiments performed under different bias fields. The temperature coefficient of the hyperfine interaction for ^{13}C(3) nuclear spins is measured under three bias fields for two NV centers.

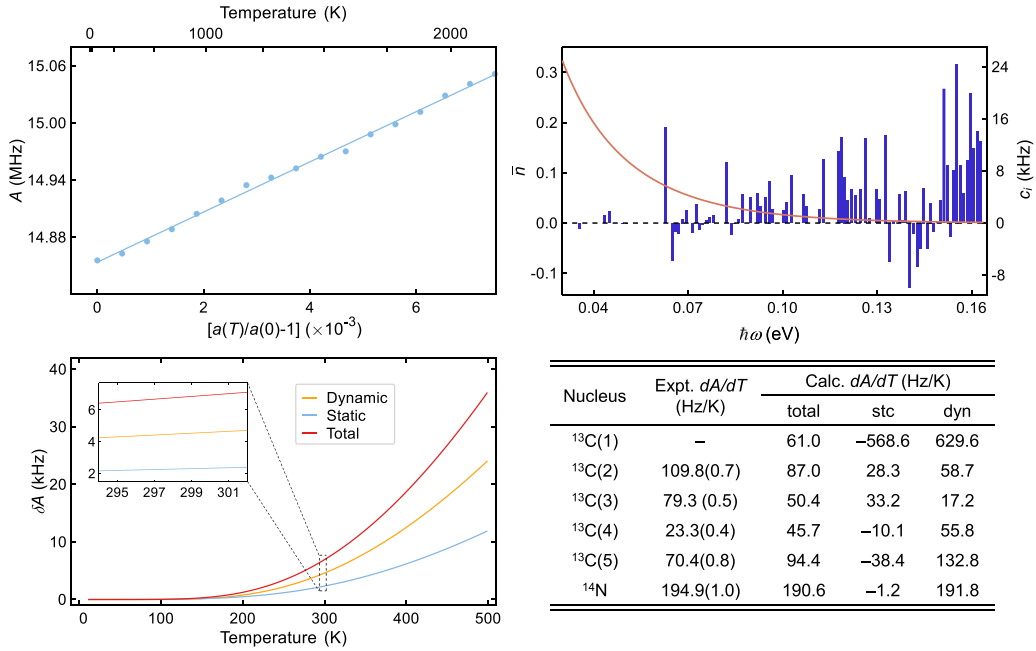

Nucleus	Expt. dA/dT (Hz/K)	Calc. dA/dT (Hz/K)		
		total	stc	dyn
^{13}C(1)	–	61.0	–568.6	629.6
^{13}C(2)	109.8(0.7)	87.0	28.3	58.7
^{13}C(3)	79.3 (0.5)	50.4	33.2	17.2
^{13}C(4)	23.3(0.4)	45.7	–10.1	55.8
^{13}C(5)	70.4(0.8)	94.4	–38.4	132.8
^{14}N	194.9(1.0)	190.6	–1.2	191.8

FIG. 4. Calculation of the temperature-dependent coupling $A(T)$. (a) Coupling strength $A = \sqrt{A_{zx}^2 + A_{zy}^2 + A_{zz}^2}$ for the ^{13}C(2) spin under the thermal expansion $a(T)/a(0) - 1$ with the corresponding temperature given by the upper abscissa axis, where the tiny tick near 0 K is 250 K. It clearly shows that the static contribution $\delta A_{\rm stc}$ is proportional to the change of the lattice constant. (b) Average phonon number $\bar{n}(T) = [\exp(\hbar\omega/k_{\rm B}T) - 1]^{-1}$ at $T = 300$ K and the dynamical contribution per phonon c_i for the ^{13}C(2) spin as a function of the phonon energy $\hbar\omega$. Note that the c_i's from nearly degenerate modes (within 1 meV) are merged for display. (c) Total thermal correction $\delta A(T)$ and its composition for the ^{13}C(2) spin. Both static, i.e., thermal expansion, and dynamic, i.e., lattice vibrations, contributions are significant. (d) Comparison between the calculations and the experimental results at room temperature on the temperature dependence of the parameters regarding the nearby nuclear spins. The last two columns represent the contributions from thermal expansion (stc) and lattice vibrations (dyn). All errors in parentheses stand for one standard deviation.

calculations, $4 \times 4 \times 4$ supercells are adopted to represent the NV$^-$ centers. The vibration modes at the Γ point and the electron-spin densities under different geometric structures are calculated with the Perdew-Burke-Ernzerhof density functional [51] and an energy cutoff of 400 eV. Here we are focusing on the calculation of the coupling term $A = \sqrt{A_{zx}^2 + A_{zy}^2 + A_{zz}^2}$ for directly comparing with the experimental results.

The temperature dependence of $A(T)$ contains two contributions, the part $\delta A_{\rm stc}(T)$ due to thermal expansion and the part $\delta A_{\rm dyn}(T)$ due to lattice vibrations, i.e.,

$$A(T) = A(0) + \delta A_{\rm stc}(T) + \delta A_{\rm dyn}(T). \tag{6}$$

The static part $\delta A_{\rm stc}(T)$ is obtained by considering the impact of the temperature-related lattice expansion, with all atoms in the supercell residing at their static equilibrium positions. Our calculations show that $\delta A_{\rm stc}(T)$, as plotted in Fig. 4(a) for the ^{13}C(2) spin as an example, is proportional to the expansion of the lattice constant $a(T)/a(0) - 1$, i.e.,

$$\delta A_{\rm stc}(T) = c_{\rm stc}\left(\frac{a(T)}{a(0)} - 1\right). \tag{7}$$

In obtaining $\delta A_{\rm stc}(T)$, the temperature-dependent relative variation of lattice constant $a(T)/a(0) - 1$ is required and has been determined by fitting experimental data in Ref. [52] (replotted in Fig. S4 in [35]). As shown by the upper abscissa of Fig. 4(a), below 1000 K, $a(T)/a(0) - 1$ is very small but increases rapidly. The coefficient $c_{\rm stc}$ is determined by linearly fitting the calculated $\delta A_{\rm stc}$ at a series of lattice expansion configurations. In order to reduce the impact of numerical errors in the first-principles calculations, a much larger range of $a(T)/a(0) - 1$ is adopted in the linear fitting.

To obtain $\delta A_{\rm dyn}(T)$, we calculated $A_{\rm stc}(X_i)$ as a function of the canonical coordinate X_i for the vibration mode $i = 1$–1530 of the supercell. The function $A_{\rm stc}(X_i)$ can be well fitted by a rank-2 polynomial as

$$A_{\rm stc}(X_i) - A_{\rm stc}(0) = b_i X_i + c_i \frac{\omega_i}{\hbar} X_i^2, \tag{8}$$

where b_i and c_i are the fitting parameters, ω_i is the phonon frequency, and $\hbar$ is the reduced Planck constant. Evaluating the thermodynamic expectation value of $A_{\rm stc}(X_i) - A_{\rm stc}(0)$ at temperature T and then summing over all the vibration modes, we obtain the expressions of $\delta A_{\rm dyn}(T)$ and $A(0)$ in Eq. (6) as

$$\delta A_{\rm dyn}(T) = \sum_i c_i \bar{n}_i(T), \tag{9}$$

$$A(0) = A_{\rm stc}(0) + \sum_i \frac{c_i}{2}, \tag{10}$$

where $\bar{n}_i(T) = [\exp(\hbar\omega_i/k_{\rm B}T) - 1]^{-1}$ is the average phonon number of the vibration mode i, with $k_{\rm B}$ the Boltzmann constant, and the fitting parameter c_i [defined in Eq. (8)] gives the contribution per phonon to $\delta A_{\rm dyn}$.

The contributions of different vibration modes and the temperature-dependent part of $A(T)$ for the ^{13}C(2) spin are

displayed in Figs. 4(b) and 4(c) (see the Supplemental Material [35] for more details in determining A_{stc} and A_{dyn}). The calculation has been done for ^{14}N and ^{13}C(1–5) spins in exactly the same way.

Figure 4(d) lists the calculated and measured temperature derivatives of $A(T)$ at 300 K for the ^{14}N and ^{13}C(1–5) spins. The calculated temperature derivatives of hyperfine coupling match the magnitude of the experimental results and reflect the trend of derivatives for different nuclei, which indicates our first-principles calculations are capable of describing such a delicate variation of hyperfine coupling with a straightforward model disregarding the higher-order terms in the temperature-dependent hyperfine coupling. At 300 K, the dynamical part dominates for the ^{14}N spin, while both the static and dynamical terms contribute significantly to various ^{13}C spins. In addition, the temperature-dependent terms are always much smaller than their corresponding $A(0)$ in magnitude (approximately 1% for the ^{14}N spin and the scale of 0.01%–0.1% for the ^{13}C spins at 300 K), which confirms the weak coupling between the lattice deformation and the hyperfine interaction.

V. CONCLUSION

The temperature coefficients of the temperature-dependent parameters contained in the ground-state Hamiltonian of single NV^- centers were precisely measured at room temperature and first-principles calculations explained the experimental results fairly well. In particular, the temperature coefficients of the quadrupole coupling of the ^{14}N nuclear spin and the hyperfine interactions of the ^{14}C and ^{13}C spins were measured with hertz-level precision by performing Ramsey interferometry on the nuclear spins. Among these parameters, the hyperfine coupling of the ^{14}N spin has the largest susceptibility to the temperature. Thus, it may work as a nanoscale thermometer like the ZFS [11,12,19], considering that millisecond-scale coherence times can nearly remedy the gap in the temperature coefficient compared to the ZFS.

In the future, it would be worthwhile to perform the measurements with varying strains or a wider range of temperatures for allowing a more detailed test of the calculation results. The calculations can be further improved by adopting a more accurate description of the NV^- such as a larger supercell and a more accurate density functional, a higher-precision response of the variation of the spin-density function to tiny structure changes, and a more thorough description of the anharmonic effect. The methods for high-precision measurements and first-principles calculations in this work are universal and can help deepen our understanding of NV centers as well as other solid-state defects [30–33].

Source data for all figures in the text and Supplemental Material are available from the corresponding authors upon reasonable request.

ACKNOWLEDGMENTS

This work was supported by the National Key R&D Program of China (Grants No. 2018YFA0306600 and No. 2016YFA0502400), the National Natural Science Foundation of China (Grants No. 81788101, No. 91636217, No. T2125011, and No. 12274396), Innovation Program for Quantum Science and Technology (Grants No. 2021ZD0302200 and No. 2021ZD0303204), the CAS (Grants No. XDC07000000, No. GJJSTD20200001, No. QYZDY-SSW-SLH004, and No. Y201984), the Anhui Initiative in Quantum Information Technologies (Grant No. AHY050000), the CAS Project for Young Scientists in Basic Research, the Fundamental Research Funds for the Central Universities, the China Postdoctoral Science Foundation (Grants No. 2021M703110 and No. 2022T150631), and the Hefei Comprehensive National Science Center. The numerical calculations were performed on the supercomputing system at the Supercomputing Center of University of Science and Technology of China.

[1] G. Wolfowicz, F. J. Heremans, C. P. Anderson, S. Kanai, H. Seo, A. Gali, G. Galli, and D. D. Awschalom, Quantum guidelines for solid-state spin defects, Nat. Rev. Mater. **6**, 906 (2021).

[2] C. L. Degen, F. Reinhard, and P. Cappellaro, Quantum sensing, Rev. Mod. Phys. **89**, 035002 (2017).

[3] D. D. Awschalom, R. Hanson, J. Wrachtrup, and B. B. Zhou, Quantum technologies with optically interfaced solid-state spins, Nat. Photon. **12**, 516 (2018).

[4] M. W. Doherty, N. B. Manson, P. Delaney, F. Jelezko, J. Wrachtrup, and L. C. L. Hollenberg, The nitrogen-vacancy colour centre in diamond, Phys. Rep. **528**, 1 (2013).

[5] F. Shi, Q. Zhang, P. Wang, H. Sun, J. Wang, X. Rong, M. Chen, C. Ju, F. Reinhard, H. Chen *et al.*, Single-protein spin resonance spectroscopy under ambient conditions, Science **347**, 1135 (2015).

[6] I. Lovchinsky, A. O. Sushkov, E. Urbach, N. P. de Leon, S. Choi, K. De Greve, R. Evans, R. Gertner, E. Bersin, C. Müller *et al.*, Nuclear magnetic resonance detection and spectroscopy of single proteins using quantum logic, Science **351**, 836 (2016).

[7] F. Shi, F. Kong, P. Zhao, X. Zhang, M. Chen, S. Chen, Q. Zhang, M. Wang, X. Ye, Z. Wang *et al.*, Single-DNA electron spin resonance spectroscopy in aqueous solutions, Nat. Methods **15**, 697 (2018).

[8] L. Thiel, Z. Wang, M. A. Tschudin, D. Rohner, I. Gutiérrez-Lezama, N. Ubrig, M. Gibertini, E. Giannini, A. F. Morpurgo, and P. Maletinsky, Probing magnetism in 2D materials at the nanoscale with single-spin microscopy, Science **364**, 973 (2019).

[9] M. J. H. Ku, T. X. Zhou, Q. Li, Y. J. Shin, J. K. Shi, C. Burch, L. E. Anderson, A. T. Pierce, Y. Xie, A. Hamo *et al.*, Imaging viscous flow of the Dirac fluid in graphene, Nature (London) **583**, 537 (2020).

[10] T. Song, Q.-C. Sun, E. Anderson, C. Wang, J. Qian, T. Taniguchi, K. Watanabe, M. A. McGuire, R. Stöhr, D. Xiao *et al.*, Direct visualization of magnetic domains and moiré magnetism in twisted 2D magnets, Science **374**, 1140 (2021).

[11] G. Kucsko, P. C. Maurer, N. Y. Yao, M. Kubo, H. J. Noh, P. K. Lo, H. Park, and M. D. Lukin, Nanometre-scale thermometry in a living cell, Nature (London) **500**, 54 (2013).

[12] P. Neumann, I. Jakobi, F. Dolde, C. Burk, R. Reuter, G. Waldherr, J. Honert, T. Wolf, A. Brunner, J. H. Shim *et al.*, High-precision nanoscale temperature sensing using single defects in diamond, Nano Lett. **13**, 2738 (2013).

[13] M. Pompili, S. L. N. Hermans, S. Baier, H. K. C. Beukers, P. C. Humphreys, R. N. Schouten, R. F. L. Vermeulen, M. J. Tiggelman, L. dos Santos Martins, B. Dirkse *et al.*, Realization of a multinode quantum network of remote solid-state qubits, Science **372**, 259 (2021).

[14] S. L. N. Hermans, M. Pompili, H. K. C. Beukers, S. Baier, J. Borregaard, and R. Hanson, Qubit teleportation between non-neighbouring nodes in a quantum network, Nature (London) **605**, 663 (2022).

[15] V. M. Acosta, E. Bauch, M. P. Ledbetter, A. Waxman, L.-S. Bouchard, and D. Budker, Temperature Dependence of the Nitrogen-Vacancy Magnetic Resonance in Diamond, Phys. Rev. Lett. **104**, 070801 (2010).

[16] X.-D. Chen, C.-H. Dong, F.-W. Sun, C.-L. Zou, J.-M. Cui, Z.-F. Han, and G.-C. Guo, Temperature dependent energy level shifts of nitrogen-vacancy centers in diamond, Appl. Phys. Lett. **99**, 161903 (2011).

[17] D. M. Toyli, D. J. Christle, A. Alkauskas, B. B. Buckley, C. G. Van de Walle, and D. D. Awschalom, Measurement and Control of Single Nitrogen-Vacancy Center Spins above 600 K, Phys. Rev. X **2**, 031001 (2012).

[18] M. W. Doherty, V. M. Acosta, A. Jarmola, M. S. J. Barson, N. B. Manson, D. Budker, and L. C. L. Hollenberg, Temperature shifts of the resonances of the NV^- center in diamond, Phys. Rev. B **90**, 041201(R) (2014).

[19] D. M. Toyli, C. F. de Las Casas, D. J. Christle, V. V. Dobrovitski, and D. D. Awschalom, Fluorescence thermometry enhanced by the quantum coherence of single spins in diamond, Proc. Natl. Acad. Sci. USA **110**, 8417 (2013).

[20] M. S. J. Barson, P. Reddy, S. Yang, N. B. Manson, J. Wrachtrup, and M. W. Doherty, Temperature dependence of the ^{13}C hyperfine structure of the negatively charged nitrogen-vacancy center in diamond, Phys. Rev. B **99**, 094101 (2019).

[21] V. V. Soshenko, V. V. Vorobyov, S. V. Bolshedvorskii, O. Rubinas, I. Cojocaru, B. Kudlatsky, A. I. Zeleneev, V. N. Sorokin, A. N. Smolyaninov, and A. V. Akimov, Temperature drift rate for nuclear terms of the NV-center ground-state Hamiltonian, Phys. Rev. B **102**, 125133 (2020).

[22] A. Jarmola, I. Fescenko, V. M. Acosta, M. W. Doherty, F. K. Fatemi, T. Ivanov, D. Budker, and V. S. Malinovsky, Robust optical readout and characterization of nuclear spin transitions in nitrogen-vacancy ensembles in diamond, Phys. Rev. Res. **2**, 023094 (2020).

[23] G. Wang, A. R. Barr, H. Tang, M. Chen, C. Li, H. Xu, J. Li, and P. Cappellaro, Characterizing temperature and strain variations with qubit ensembles for their robust coherence protection, arXiv:2205.02790.

[24] A. Gali, M. Fyta, and E. Kaxiras, *Ab initio* supercell calculations on nitrogen-vacancy center in diamond: Electronic structure and hyperfine tensors, Phys. Rev. B **77**, 155206 (2008).

[25] A. Ranjbar, M. Babamoradi, M. Heidari Saani, M. A. Vesaghi, K. Esfarjani, and Y. Kawazoe, Many-electron states of nitrogen-vacancy centers in diamond and spin density calculations, Phys. Rev. B **84**, 165212 (2011).

[26] J. R. Maze, A. Gali, E. Togan, Y. Chu, A. Trifonov, E. Kaxiras, and M. D. Lukin, Properties of nitrogen-vacancy centers in diamond: The group theoretic approach, New J. Phys. **13**, 025025 (2011).

[27] M. W. Doherty, F. Dolde, H. Fedder, F. Jelezko, J. Wrachtrup, N. B. Manson, and L. C. L. Hollenberg, Theory of the ground-state spin of the NV^- center in diamond, Phys. Rev. B **85**, 205203 (2012).

[28] Á. Gali, *Ab initio* theory of the nitrogen-vacancy center in diamond, Nanophotonics **8**, 1907 (2019).

[29] H. Tang, A. R. Barr, G. Wang, P. Cappellaro, and J. Li, First-principles calculation of the temperature-dependent transition energies in spin defects, arXiv:2205.02791.

[30] M. T. Mądzik, S. Asaad, A. Youssry, B. Joecker, K. M. Rudinger, E. Nielsen, K. C. Young, T. J. Proctor, A. D. Baczewski, A. Laucht *et al.*, Precision tomography of a three-qubit donor quantum processor in silicon, Nature (London) **601**, 348 (2022).

[31] M. Widmann, S.-Y. Lee, T. Rendler, N. T. Son, H. Fedder, S. Paik, L.-P. Yang, N. Zhao, S. Yang, I. Booker *et al.*, Coherent control of single spins in silicon carbide at room temperature, Nat. Mater. **14**, 164 (2015).

[32] P. Siyushev, K. Xia, R. Reuter, M. Jamali, N. Zhao, N. Yang, C. Duan, N. Kukharchyk, A. D. Wieck, R. Kolesov *et al.*, Coherent properties of single rare-earth spin qubits, Nat. Commun. **5**, 3895 (2014).

[33] A. Ruskuc, C.-J. Wu, J. Rochman, J. Choi, and A. Faraon, Nuclear spin-wave quantum register for a solid-state qubit, Nature (London) **602**, 408 (2022).

[34] T. Xie, Z. Zhao, X. Kong, W. Ma, M. Wang, X. Ye, P. Yu, Z. Yang, S. Xu, P. Wang *et al.*, Beating the standard quantum limit under ambient conditions with solid-state spins, Sci. Adv. **7**, eabg9204 (2021).

[35] See Supplemental Material at http://link.aps.org/supplemental/10.1103/PhysRevB.107.L140101 for additional details on experimental methods, experimental results, and first-principles calculations, which include additional Refs. [36–45].

[36] L. Childress, M. V. Gurudev Dutt, J. M. Taylor, A. S. Zibrov, F. Jelezko, J. Wrachtrup, P. R. Hemmer, and M. D. Lukin, Coherent dynamics of coupled electron and nuclear spin qubits in diamond, Science **314**, 281 (2006).

[37] V. Jacques, P. Neumann, J. Beck, M. Markham, D. Twitchen, J. Meijer, F. Kaiser, G. Balasubramanian, F. Jelezko, and J. Wrachtrup, Dynamic Polarization of Single Nuclear Spins by Optical Pumping of Nitrogen-Vacancy Color Centers in Diamond at Room Temperature, Phys. Rev. Lett. **102**, 057403 (2009).

[38] M. Steiner, P. Neumann, J. Beck, F. Jelezko, and J. Wrachtrup, Universal enhancement of the optical readout fidelity of single electron spins at nitrogen-vacancy centers in diamond, Phys. Rev. B **81**, 035205 (2010).

[39] P. E. Blöchl, First-principles calculations of defects in oxygen-deficient silica exposed to hydrogen, Phys. Rev. B **62**, 6158 (2000).

[40] O. V. Yazyev, I. Tavernelli, L. Helm, and U. Röthlisberger, Core spin-polarization correction in pseudopotential-based electronic structure calculations, Phys. Rev. B **71**, 115110 (2005).

[41] P. E. Blöchl, Projector augmented-wave method, Phys. Rev. B **50**, 17953 (1994).

[42] G. Kresse and J. Hafner, *Ab initio* molecular dynamics for liquid metals, Phys. Rev. B **47**, 558 (1993).

[43] G. Kresse and J. Hafner, *Ab initio* molecular-dynamics simulation of the liquid-metal–amorphous-semiconductor transition in germanium, Phys. Rev. B **49**, 14251 (1994).

[44] http://nmrwiki.org/wiki/index.php?title=Gyromagnetic_ratio.

[45] T. Sato, K. Ohashi, T. Sudoh, K. Haruna, and H. Maeta, Thermal expansion of a high purity synthetic diamond single crystal at low temperatures, Phys. Rev. B **65**, 092102 (2002).

[46] T. Xie, Z. Zhao, M. Guo, M. Wang, F. Shi, and J. Du, Identity Test of Single NV^- Centers in Diamond at Hz-Precision Level, Phys. Rev. Lett. **127**, 053601 (2021).

[47] A. Gali, Identification of individual ^{13}C isotopes of nitrogen-vacancy center in diamond by combining the polarization studies of nuclear spins and first-principles calculations, Phys. Rev. B **80**, 241204(R) (2009).

[48] B. Smeltzer, L. Childress, and A. Gali, ^{13}C hyperfine interactions in the nitrogen-vacancy centre in diamond, New J. Phys. **13**, 025021 (2011).

[49] J. H. Shim, B. Nowak, I. Niemeyer, J. Zhang, F. D. Brandao, and D. Suter, Characterization of hyperfine interaction between single electron and single nuclear spins in diamond assisted by quantum beat from the nuclear spin, arXiv:1307.0257.

[50] J. D. Jackson, *Classical Electrodynamics* (Wiley, New York, 1998), Chap. 5, Sec. VI, p. 188.

[51] J. P. Perdew, K. Burke, and M. Ernzerhof, Generalized Gradient Approximation Made Simple, Phys. Rev. Lett. **77**, 3865 (1996).

[52] P. Jacobson and S. Stoupin, Thermal expansion coefficient of diamond in a wide temperature range, Diamond Relat. Mater. **97**, 107469 (2019).